WILEY-VCH

Analysis of Leakage Channel with Different Al composition Back-Barrier in AlN/GaN High Electron Mobility Transistor on Si

Siyu Liu,[1,2,] Yihao Zhuang,[1] Hanchao Li,[2] Pengju Cui,[2] Qingyun Xie,[3,4] Yue Wang,[5] Hanlin Xie,[3,4] Kumud Ranjan,[3,4] Geok Ing Ng[1,2,3,4,5,*]*

[1]*Energy Research Institute, Nanyang Technological University, 1 CleanTech Loop, #06-04, Singapore 637141, Republic of Singapore*

[2]*School of Electrical and Electronic Engineering, Nanyang Technological University, 50 Nanyang Avenue, Singapore 639798, Republic of Singapore*

[3]*National GaN Technology Centre (NGTC), Agency for Science, Technology and Research (A*STAR), Innovis #08-02, Singapore 138634, Republic of Singapore*

[4]*Institute of Microelectronics (IME), Agency for Science, Technology and Research (A*STAR), Innovis #08-02, Singapore 138634, Republic of Singapore*

[5]*Low Energy Electronic Systems, Singapore-MIT Alliance for Research and Technology, 1 CREATE Way, #10-01 CREATE Tower, Singapore 138602, Republic of Singapore*

E-mail: sy.liu@ntu.sdu.sg, eging@ntu.edu.sg

Keywords: GaN HEMTs, parasitic channel, off-state leakage, back-barrier, Al composition

Abstract

This study investigates the effect of different Al compositions in the back-barrier (BB) materials on the off-state leakage characteristics of AlN/GaN/Al_xGaN high electron mobility transistors (HEMTs) on Si substrates. The position of the N-type parasitic channel within the epitaxial material is further validated. Electrical performance measurements of AlN/GaN/AlGaN HEMTs with varying isolation depths are conducted, and parasitic channels in the unintentionally doped AlGaN BB are confirmed through isolation leakage and capacitance tests. TLM results reveal that the parasitic channel is an N-type channel with a sheet resistance of 7078.4 Ω/sq. Simulations show that the Al composition in the BB layer influences the position of the N-type parasitic channel. As the Al composition increases to 15%, the parasitic channel contracts from the BB layer into the GaN channel layer. Isolation leakage tests on $Al_{0.2}$GaN and AlN BBs, with the isolation depth controlled at the interface between the channel and the BB layers, yield leakage currents of 3.9×10^{-4} mA/mm and 2×10^{-7} mA/mm, respectively.

1. Introduction

AlN/GaN on silicon substrate technology has attracted significant attention for its excellent performance in high-frequency, high-voltage, and high-temperature applications, positioning it as a key enabler for millimeter-wave communication systems.[1–3] The excellent material properties of AlN/GaN HEMTs offer great advantages in high power density and efficiency. Furthermore, the introduction of the AlGaN back-barrier (BB) layer not only enhances the carrier confinement in the two-dimensional electron gas (2DEG) but also significantly improves the breakdown voltage and robustness of device.[4,5] However, despite substantial progress in cost reduction, process compatibility, and performance enhancement, the reliability of devices remains a critical challenge that limits the widespread application of silicon-based AlN/GaN technology[6,7].

Existing silicon-based AlN/GaN HEMTs technology, while achieving high performance, also presents significant limitations. The polarization effect in the AlN/GaN heterostructure is particularly pronounced, leading to a degradation in the sub-threshold characteristics [8] of RF devices and significantly reducing electron mobility.[9] Although the introduction of the AlGaN BB improves carrier confinement in the two-dimensional electron gas (2DEG) and enhances the electric field distribution, the double heterostructure (AlN/GaN/BB) may also introduce a series of issues.[10–16] For instance, the BB layer may form parasitic channels at the isolation region sidewalls, causing carriers to accumulate and flow along unintended paths, thereby affecting the turn-off performance of device.[7], [17]Additionally, the Al composition distribution in the BB plays a crucial role in the effectiveness of electron confinement, and improper composition design can lead to increased band discontinuities, thereby raising the risk of parasitic channel formation.

To address the limitations outlined above, this study combines systematic experiments and simulations to deeply analyze the formation mechanism of parasitic channels and their impact on device performance. Different etching depths were employed in the experiments, revealing that parasitic channels primarily form at the interface between the BB layer and the sidewalls of the isolation region. Electron transport through the parasitic channels occurs via the two-dimensional variable range hopping (2D-VRH) mechanism, where electrons jump between localized states over a variable distance. This mechanism becomes dominant in regions with disorder or defects, such as at the interface or sidewalls of the isolation region. Electrons can flow through the parasitic channel even in the off-state, leading to abnormal leakage currents.[7] Transmission Line Model (TLM) measuring indicated that the sheet resistance of the parasitic channel is 7087.4 Ω/sq, with a saturation current of 13 mA/mm. Furthermore, band structure simulations and experimental validation of devices with varying Al compositions in the BB revealed that optimized Al composition design significantly improves carrier confinement in the BB and effectively suppresses the formation of parasitic channels. The innovation of this study lies in uncovering the formation mechanism of parasitic channels and providing guidance for optimizing BB design, offering new insights for improving the reliability and expanding the application of silicon-based AlN/GaN HEMTs.

2. Experimental Section

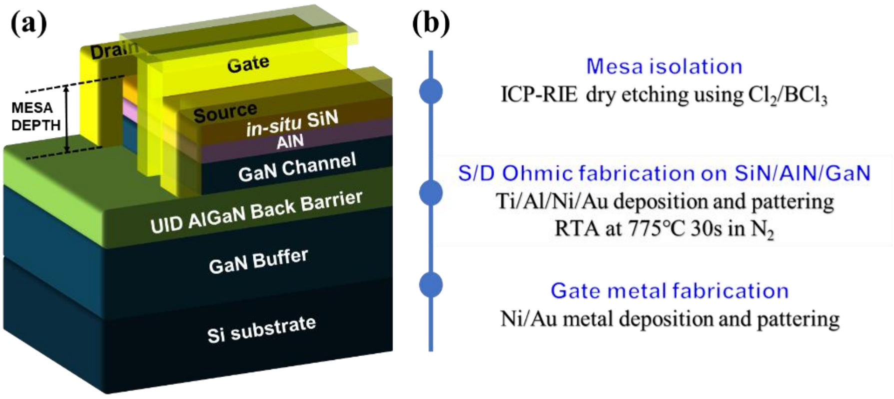

Figure 1. Schematic of the cross section and Fabrication flow of the AlN/GaN HEMTs on Si.

Figure 1(a) shows the cross-sectional schematic of AlN/GaN HEMTs fabricated on a Si substrate using metal organic chemical vapor deposition. From bottom to top of the epitaxial structure, comprises a high-resistivity Si substrate, a GaN buffer layer, a 250 nm $Al_{0.08}GaN$ BB layer, an 80 nm GaN channel layer, a 4 nm AlN barrier layer, and a 3 nm *in-situ* SiN layer. Hall measurements reveal a sheet carrier density of 1.47×10^{13} cm^{-2}, a mobility of 1075 cm^2/V, and a sheet resistance of 395 Ω/sq. Figure 1(b) outlines the fabrication process. Initially, mesas were formed using ICP-RIE, with their position and depth shown in Figure 1(a). Subsequently, Ti/Al/Ni/Au alloy ohmic contacts were deposited via E-beam evaporation and annealed at 775 °C for 30 seconds in an N_2 atmosphere, achieving a contact resistance (R_c) of 0.33 Ω·mm. Finally, the suspended T-gate structure was defined using a bilayer photoresist, followed by Ni/Au deposition to form the T-shaped gate. The fabricated device features a source-drain spacing of 3 µm and a gate length of 120 nm.

3. Results and Discussions

3.1. DC characteristics, Isolation leakage, C-V and Transmission Line Model (TLM)

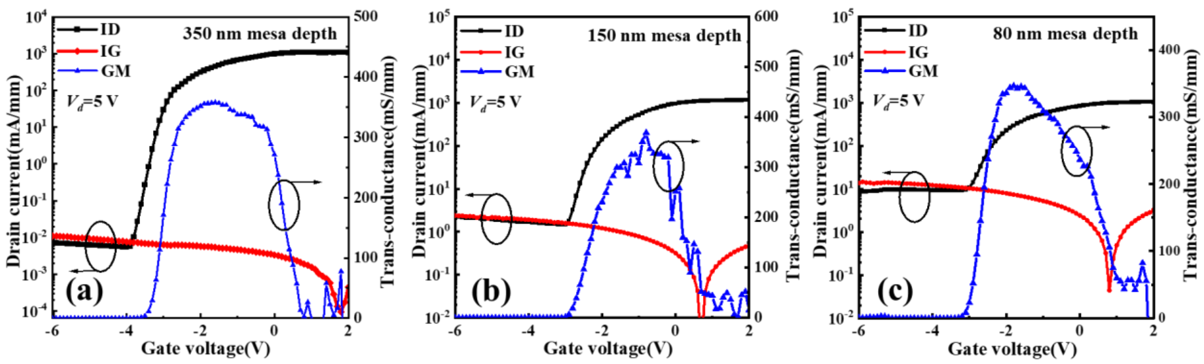

Figure 2. Transfer sweeps and gate current curves of the AlN/GaN HEMTs on Si with different depth of mesa.

Figure 2 shows the transfer characteristics of AlN/GaN HEMTs with three different mesa isolation depths: 80 nm, 150 nm, and 350 nm. The gate voltage ranges from -6 V to 2 V, with a drain bias fixed at 5 V. All devices feature a L_G of 120 nm and an L_{SD} of 3 µm. The structure with a mesa depth of 350 nm exhibits a normal off-state leakage current of 7.1 × 10^{-3} mA/mm. In contrast, the off-state leakage currents for the 150 nm and 80 nm mesa depths are abnormally high, measuring 2.2 mA/mm and 9.6 mA/mm, respectively. Although these three devices exhibit almost identical saturation current and transconductance values, the off-state leakage current decreases with increasing mesa depth, eventually stabilizing at a normal level at a depth of 350 nm. This indicates that the primary difference between these structures lies in their off-state leakage behavior. This is due to the leakage path present in the MESA region, which is related to the etching depth; a 350 nm etching depth effectively blocks this leakage channel and reduces the leakage current.

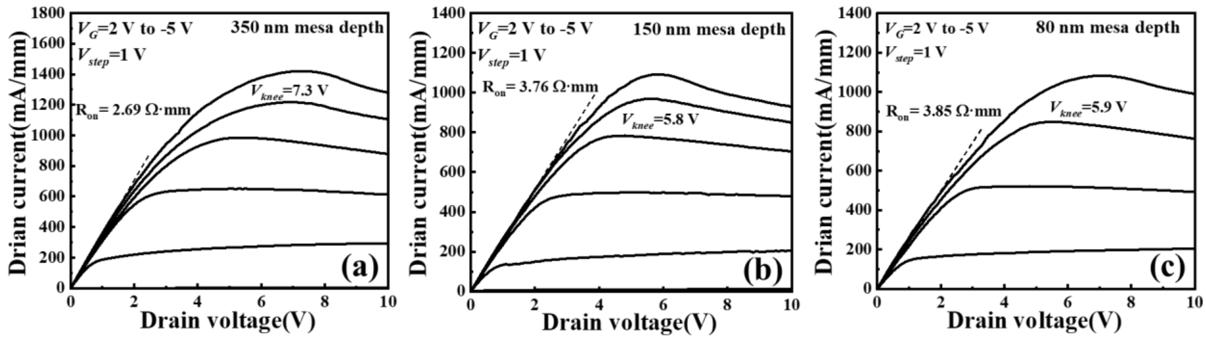

Figure 3. Output curves of the AlN/GaN HEMTs on Si with different depth of mesa.

Figure 3 presents the output characteristics of devices with three different mesa depths, with gate voltages ranging from -5 V to 2 V and drain voltages from 0 V to 10 V. As the mesa depth decreases, R_{on} is increased from 2.69 Ω·mm to 3.85 Ω·mm. It is observed that the current is uniformly reduced with decreasing gate voltage; however, devices with mesa depths of 150 nm and 80 nm are not fully turned off, and slight leakage currents are detected. These leakage currents are found to increase with higher drain voltages, indicating that the leakage channel is not fully depleted by the gate. This observation is consistent with our earlier findings, where parasitic channel leakage was identified in the BB layer and found to be difficult to deplete completely.

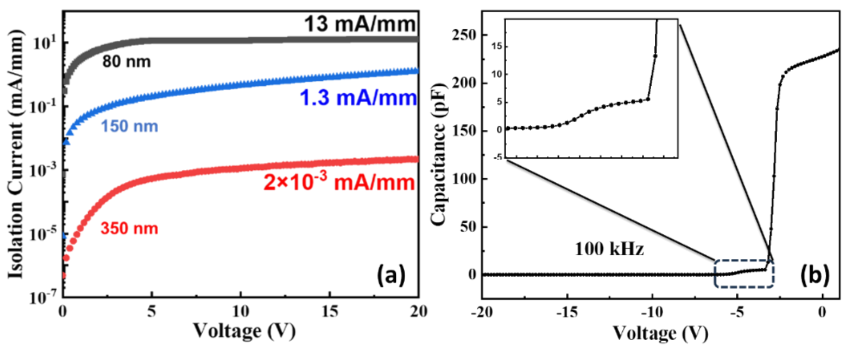

Figure 4. (a) Isolation leakage at 80, 150 and 350 nm isolation depths. (b) *C-V* characteristics at 100 kHz frequency.

To verify whether the leakage current in the devices is primarily caused by parasitic channels, isolation leakage tests were performed on devices with three different mesa depth structures. Figure 4 (a) shows the leakage current in the isolation region under voltages ranging from 0 to 20 V. The structure with a mesa depth of 350 nm exhibits normal isolation leakage of 2×10^{-3} mA/mm, while the device with an 80 nm mesa depth shows abnormal isolation leakage exceeding 10 mA/mm. For the device with a 150 nm mesa depth, the leakage current is reduced by an order of magnitude compared to the 80 nm structure but remains at 1.3 mA/mm. This persistent leakage reveals the cause of the abnormal DC off-state characteristics, as the properties of the parasitic channel allow leakage to be detected even in the passive region. The parasitic channel forms due to the incomplete isolation in the MESA region, where carriers accumulate and flow along unintended paths, bypassing the main conduction channel. This leads to off-state leakage, which occurs through the two-dimensional variable range hopping (2D-VRH) mechanism, where electrons hop between localized states in the parasitic channel, allowing current to flow even when the device is in the off-state. As shown in Figure 4(b), the capacitance characteristics of the device were tested using a *C-V* loop structure. The voltage range for testing was defined from -20 V to 1 V, with a scanning frequency of 100 kHz. From the inset, it can be observed that, unlike the single heterojunction device, there is a small step in capacitance at -6 V, which provides evidence for the existence of a parasitic channel, and it is identified as an N-type channel.

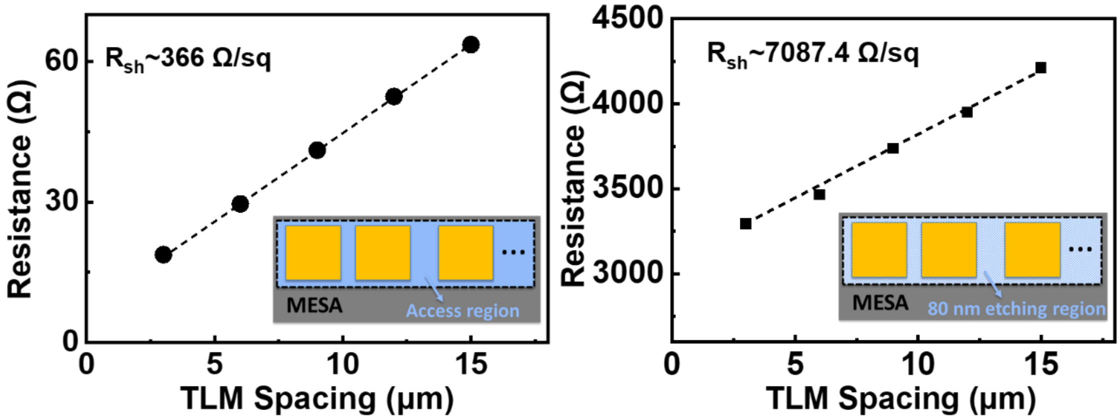

Figure 5. TLM measurement of various TLM structures with a 350 nm mesa depth.

To confirm the presence of the N-type parasitic channel, in addition to the conventional TLM structure with a 350 nm mesa depth, a "non-2DEG TLM structure" was also fabricated, where the access region between the ohmic contacts in the TLM structure was etched to a depth of 80 nm. The measurement results, shown in Figure 5, validate the presence of the parasitic channel in this device, with illustrations depicting the different test structures. For the conventional TLM structure with a 350 nm mesa depth, the measured sheet resistance was 366 Ω/sq. However, the TLM structure with the same mesa depth but with the access region etched to 80 nm showed a significantly higher sheet resistance of 7087.4 Ω/sq, indicating the presence of a leakage path. This suggests that even after eliminating the influence of the 2DEG, a parasitic channel with properties similar to those of the 2DEG remains below the epitaxial material at a depth of 80 nm, thus confirming the existence of the parasitic channel.

3.2. Band structure, simulation results, and analysis

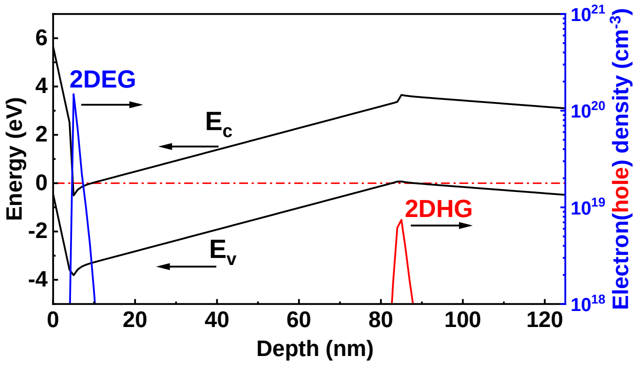

Figure 6. The energy band diagram under ideal conditions is calculated through the one-dimensional Poisson equation.

The one-dimensional Poisson equation was employed to compute the energy band and electron concentration of the material structure, with the findings presented in Figure 6. At the interface between the AlN barrier layer and the GaN channel layer, a 2DEG channel is observed. Additionally, we identified a parasitic 2DHG channel with a low electron concentration at the interface between the GaN channel and the AlGaN BB. However, previous TLM measurements indicated that the existing parasitic channel is an N-type channel with a sheet resistance of approximately 7000 Ω/sq. Another contributing factor is that the ohmic contact pads used in the experiment are N-type, which do not effectively connect to the P-type channel. Therefore, the existing parasitic channel is primarily an N-type channel dominated by electron conduction.

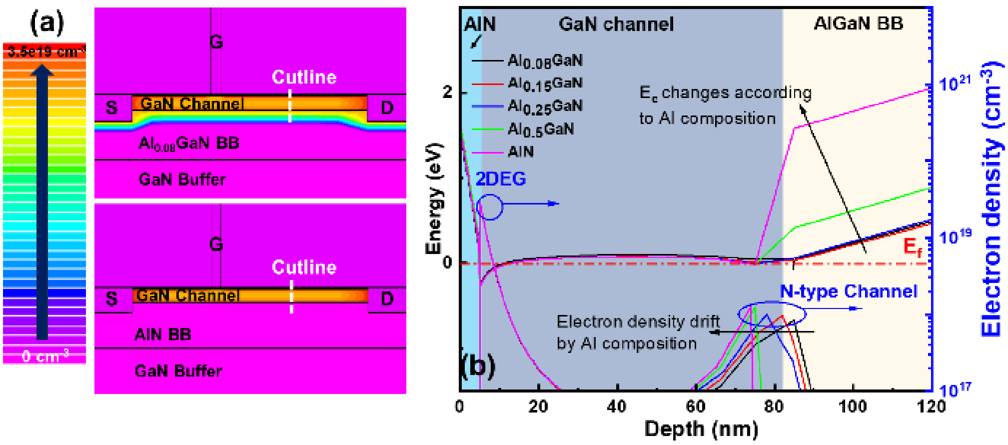

Figure 7. (a) The electron concentration gradient distribution diagram after simulating the $Al_{0.08}$GaN BB structure and AlN under the polarization model by Silvaco. (b) Changes in Ec and Electron density under the influence of BB with different Al composition.

Figure 7(a) presents a simulation of the HEMTs structure. For the $Al_{0.08}GaN$ BB structure, strong polarization failed to effectively confine electrons below the barrier layer, with some electrons surpassing the AlGaN BB. In contrast, no electrons surpassed the surface of AlN BB structure. A similar phenomenon has also been observed in previously reported studies.[18] Figure 7(b) illustrates the impact of different Al compositions in the BB on the energy band structure and electron concentration. As the Al composition increases, the energy band structure approximates the theoretical scenario (Figure 6), and the N-type leakage channel shifts from the BB into the GaN channel layer. The low Al composition in the BB explains the anomalous off-state leakage.

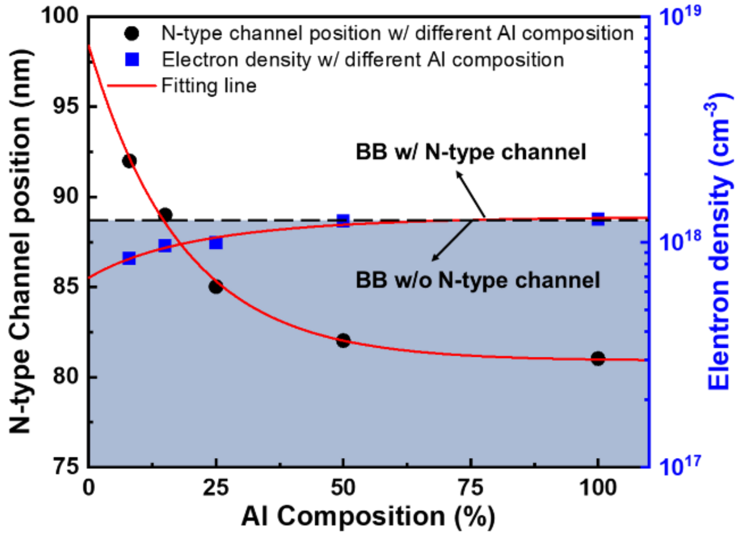

Figure 8. N-type channel position in GaN Channel and BB with different Al composition. Electron density in GaN Channel and BB with different Al composition.

Through simulation of various Al compositions, the relationship between the N-type parasitic channel and its electron concentration was determined, as shown in Figure 8. The lower Al content in the BB layer accounts for the anomalous off-state leakage behavior. It can be observed that when the Al composition in the BB ranges from 0% to 15%, the electron concentration in the N-type parasitic channel is approximately 10^{18} cm^{-3} and is confined within the BB layer. As the Al composition increases, the depth of the parasitic channel gradually shifts toward the interface between the GaN channel and the BB. When the Al composition in the BB reaches 15%, the N-type parasitic channel is located at the interface between the GaN channel and the BB layer. Further increasing the Al composition in the BB restricts the N-type parasitic channel to the GaN channel layer. However, the electrons in the parasitic channel do not dissipate immediately within the BB; instead, their concentration decreases gradually with depth. Furthermore, it is observed that the electron concentration in the N-type leakage channel is relatively unaffected by the Al composition in the BB, which helps explain the anomalous leakage observed for a mesa depth of 150 nm.

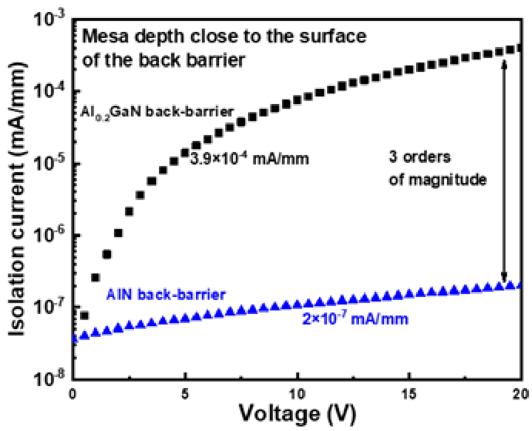

Figure 9. Isolation leakage of AlN/GaN HEMTs with different Al composition BB.

To validate the simulation model, we performed leakage testing on isolation regions with different Al compositions in the BB. The mesa etching depth was controlled at the interface between the GaN channel layer and the BB layer. As shown in the figure, the leakage current in the isolation region of $Al_{0.2}GaN$ increases with voltage, rising from 10^{-7} mA/mm to 10^{-4} mA/mm, whereas the leakage current in the AlN BB remains almost unchanged, maintaining a value of approximately 10^{-7} mA/mm. It can be observed that, with increasing Al composition, the leakage current in the isolation region gradually decreases under high electric fields. This demonstrates that increasing the Al composition can effectively suppress the formation of the N-type parasitic channel. However, considering the trade-off between growth quality and Al composition, it is necessary to carefully select an appropriate Al content in the BB, depending on the polarization strength. While higher Al content enhances carrier confinement and reduces parasitic channel formation, excessive Al can cause lattice mismatch and material defects, negatively impacting device performance. Thus, an optimal Al composition should be selected to balance parasitic channel suppression with material quality and device reliability.

4. Conclusion

In conclusion, this work combines experimental results and simulation analysis to demonstrate that isolation leakage in AlN/GaN HEMTs is strongly influenced by the Al composition in the BB. Specifically, variations in Al composition not only affect the effectiveness of carrier confinement but also play a crucial role in mitigating the formation of parasitic channels. The study highlights that improper Al composition can exacerbate leakage currents, while an optimized Al distribution can significantly enhance device performance by improving carrier confinement, reducing leakage, and maintaining robust switching characteristics. These findings provide valuable insights and practical guidelines for the design and fabrication of next-generation GaN HEMTs, paving the way for more reliable and efficient devices with advanced BB engineering tailored for high-frequency and high-power applications.

Acknowledgements

This work is supported by the National Research Foundation (NRF) and Agency for Science, Technology and Research (A*STAR) Singapore, under the RIE2025 Manufacturing, Trade & Connectivity (MTC) Industry Alignment Fund Pre-Positioning (IAF-PP) (Grant No. M22L3a0112). This work is also supported by NRF and A*STAR under the RIE2025 White Space-MTC funding (Grant No. M23WSNG001).

Received: ((will be filled in by the editorial staff))
Revised: ((will be filled in by the editorial staff))
Published online: ((will be filled in by the editorial staff))

References

[1] H. Li, H. Xie, Q. Xie, S. Liu, Y. Wang, Y. Wang, K. Ranjan, Y. Zhuang, X. Gong, G. Ing Ng, *IEEE Electron Device Lett.* **2024**, *45*, 2315.

[2] H. Du, Z. Liu, L. Hao, W. Xing, H. Zhou, S. Zhao, J. Zhang, Y. Hao, *IEEE Electron Device Lett.* **2023**, *44*, 911.

[3] S. Liu, J. Zhu, J. Guo, K. Cheng, M. Mi, L. Qin, J. Liu, F. Jia, H. Lu, X. Ma, Y. Hao, *IEEE Electron Device Lett.* **2022**, *43*, 1621.

[4] A. Shanbhag, F. Grandpierron, K. Harrouche, F. Medjdoub, *Applied Physics Letters* **2023**, *123*, 142102.

[5] J.-G. Kim, C. Cho, E. Kim, J. S. Hwang, K.-H. Park, J.-H. Lee, *IEEE Trans. Electron Devices* **2021**, *68*, 1513.

[6] F. Medjdoub, N. Waldhoff, M. Zegaoui, B. Grimbert, N. Rolland, P. A. Rolland, *IEEE Electron Device Lett.* **2011**, *32*, 1230.

[7] S. Liu, Y. Zhuang, H. Li, Q. Xie, Y. Wang, H. Xie, K. Ranjan, G. I. Ng, *Applied Physics Letters* **2024**, *125*, 023504.

[8] H. Lu, L. Yang, B. Hou, M. Zhang, M. Wu, X.-H. Ma, Y. Hao, *Applied Physics Letters* **2022**, *120*, 173502.

[9] Y. Cao, D. Jena, *Applied Physics Letters* **2007**, *90*, 182112.

[10] J. M. All Abbas, G. Atmaca, P. Narin, E. Kutlu, B. Sarikavak-Lisesivdin, S. B. Lisesivdin, *Journal of Elec Materi* **2017**, *46*, 5278.

[11] A. Bairamis, Ch. Zervos, A. Adikimenakis, A. Kostopoulos, M. Kayambaki, K. Tsagaraki, G. Konstantinidis, A. Georgakilas, *Appl. Phys. Lett.* **2014**, *105*, 113508.

[12] D. S. Lee, X. Gao, S. Guo, T. Palacios, *IEEE Electron Device Lett.* **2011**, *32*, 617.

[13] D. S. Lee, X. Gao, S. Guo, D. Kopp, P. Fay, T. Palacios, *IEEE Electron Device Lett.* **2011**, *32*, 1525.

[14] M. Sharma, R. Chaujar, in *2020 IEEE VLSI DEVICE CIRCUIT AND SYSTEM (VLSI DCS)*, IEEE, Kolkata, India **2020**, pp. 154–158.

[15] H. Yu, B. Parvais, U. Peralagu, R. Y. ElKashlan, R. Rodriguez, A. Khaled, S. Yadav, A. Alian, M. Zhao, N. De Almeida Braga, J. Cobb, J. Fang, P. Cardinael, A. Sibaja-Hernandez, N. Collaert, in *2022 International Electron Devices Meeting (IEDM)*, IEEE, San Francisco, CA, USA **2022**, p. 30.6.1-30.6.4.

[16] Q. Yu, C. Shi, L. Yang, H. Lu, M. Zhang, X. Zou, M. Wu, B. Hou, W. Gao, S. Wu, X. Ma, Y. Hao, *Micromachines* **2024**, *15*, 1220.

[17] J. Zhu, Y. Zhang, M. J. Uren, S. Liu, P. Wang, M. Mi, B. Hou, L. Yang, M. Kuball, X. Ma, Y. Hao, *Applied Physics Letters* **2020**, *116*, 222101.

[18] P. Murugapandiyan, S. Ravimaran, J. William, *Journal of Science: Advanced Materials and Devices* **2017**, *2*, 515.